J Solid State Electrochem (2010) 14:1755–1760
DOI 10.1007/s10008-010-1031-y

ORIGINAL PAPER

Storage performance of $LiFe_{1-x}Mn_xPO_4$ nanoplates (x=0, 0.5, and 1)

Kuppan Saravanan · Jagadese J. Vittal · M. V. Reddy · B. V. R. Chowdari · Palani Balaya

Received: 23 November 2009 / Revised: 8 February 2010 / Accepted: 12 February 2010 / Published online: 19 March 2010

Abstract Although $LiFePO_4$ (LFP) is considered to be a potential cathode material for the lithium-ion batteries, its rate performance is significantly restricted by sluggish kinetics of electrons and lithium ions. Several attempts have been made so far to improve the performance of $LiFePO_4$ by reducing the grain size, doping with aliovalent atoms, and coating conductive materials such as carbon or RuO_2. We report here synthesis of LFP nanoplates by solvothermal method, tailoring the thickness as well as carbon coverage at surfaces to explore their influence on the storage performance. Due to the fact that Li^+ ion diffuses along the *b*-axis, solvothermal method was aimed to control the thickness of nanoplates across the *b*-axis. We synthesized several nanoplates with various plate thicknesses along *b*-axis; among those, nanoplates of LFP with ~30-nm-thick *b*-axis having thin (2–5 nm) and uniform layer of carbon coating exhibits high storage capacity as well as high rate performances. Thus, a favorable morphology for $LiFePO_4$ has been achieved via solvothermal method for fast insertion/extraction of Li^+ as compared to spherical nanoparticles of carbon-coated LFP. Galvanostatic cycling shows a capacity of 164±5 mAh g^{-1} at 0.1 C rate, 100±5 mAh g^{-1} at 10 C rate, and 46±5 mAh g^{-1} at 30 C rate, with excellent capacity retention of up to 50 cycles. Further attempts have been made to synthesize $LiMnPO_4$ (LMP) as well as $Li(Fe_{1-x}Mn_x)PO_4$/C (x=0.5) nanoplates using solvothermal method. Although $LiMnPO_4$ does not exhibit high storage behavior comparable with that of $LiFePO_4$, the mixed systems have shown an impressive storage performance.

Keywords $LiFePO_4$/C · $LiFe_{1-x}Mn_xPO_4$ (x=0, 0.5 and 1) · Nanoplates · Solvothermal · Li-ion battery

Introduction

Olivine-based phosphates ($LiMPO_4$, M = Mn, Fe, Co and Ni) have been recognized as a promising family of cathode materials for lithium-ion batteries [1]. Among these, $LiFePO_4$ has attracted great attention due to a variety of advantages such as ease of synthesis, environmental benignness, low cost, and high flat potential during charge/discharge processes [2–8]. In spite of these advantages, the observed electrochemical performances of $LiFePO_4$ are found to be poor (storage capacity drops significantly at high current density) [6, 7] as $LiFePO_4$ is known to be a poor conductor of both electrons as well as ions [9–12]. It is reported based on *ab initio* [13] calculations as well as atomistic simulations [14, 15] that Li ions preferably move faster along the *b*-axis than along the *a*- or *c*-axes in the crystal with orthorhombic space group *Pnma*. On the other hand, transport measurements on single-crystalline $LiFePO_4$ by Amin et al. [11], further claims that Li^+ ionic conductivity is nearly four orders of magnitude lower than the electronic conductivity along the *b*- and *c*-axes while it is many orders of magnitude

K. Saravanan · J. J. Vittal (✉)
Department of Chemistry, National University of Singapore,
Singapore 117543, Singapore
e-mail: chmjjv@nus.edu.sg

M. V. Reddy · B. V. R. Chowdari
Department of Physics, National University of Singapore,
Singapore 117542, Singapore

P. Balaya (✉)
Department of Mechanical Engineering,
National University of Singapore,
Singapore 117574, Singapore
e-mail: mpepb@nus.edu.sg

lower along the *a*-axis. Thus, in order to achieve high rate performance, it is mandatory to reduce the grain size along the *b*- and *c*-axes if not at least along the *b*-axis so that Li ions as well as electrons are extracted from the bulk instantly. Such a criteria of having a morphology with thin *b*-axis of the $LiFePO_4$ crystallites will result in high rate performances due to fast extraction of Li^+ within the bulk while the exterior decoration of $LiFePO_4$ uses conductive materials such as carbon [16–19] or RuO_2 [7] enhances the electronic wiring among various particles. It is thus important to control the morphology of the $LiFePO_4$ crystallites to achieve favorable high rate performances.

This paper aims at presenting such a nanoarchitecture with controlled morphology in $LiFePO_4$ achieved through solvothermal synthesis route which provides feasibility of reducing the *b*-axis to the smallest possible thickness reported so far with uniform coating of carbon on the surface. We show here that the present synthetic approach enables extraction of both ions as well as electrons fast enough in LFP nanoplates, resulting in high rate performances and addresses the issues related to spherical particles exhibiting isotropic transport behavior with poor rate performances. In addition, we have synthesized nanoplates of the other member of olivine family, namely $LiMnPO_4$ and nanoplates of solid solutions of $LiFe_{0.5}Mn_{0.5}PO_4$, and evaluated their storage properties.

Experimental section

Synthesis

Carbon-coated thin nanoplates of $LiFePO_4$ were synthesized using solvothermal method. A stoichiometric mixture of starting materials, lithium dihydrogen phosphate (LiH_2PO_4, Aldrich), iron(II) oxalate dihydrate ($FeC_2O_4{\cdot}2H_2O$ Merck), and D-gluconic acid lactone ($C_6H_{10}O_6$, Aldrich), in the molar ratio of 1:1:5, respectively, were taken in the Teflon vessel; 25 mL of ethylene glycol was added and sealed tightly in a stainless-steel autoclave. The autoclave was heated to 250 °C for 8 h in an oven, and then it was allowed to cool down to ambient temperature. The black precipitates obtained were washed several times with ethanol and dried. Here D-gluconic acid lactone acts as carbon source, resulting in a uniform carbon coating on $LiFePO_4$. Under a similar condition, $MnCO_3$ (Merck) was used to synthesize $LiMnPO_4$, and in case of $LiFe_{0.5}Mn_{0.5}PO_4$, $MnCO_3$ and $FeC_2O_4{\cdot}2H_2O$ were used in an equimolar ratio. As-synthesized $LiFe_{1-x}Mn_xPO_4$/C was annealed at 450 °C for 4 h in an Ar–H_2 (95:5) atmosphere in order to carbonize the gluconic acid lactone completely and to increase the crystallinity of the samples. Carbon (10 wt.%) was found from the thermogravimetric and elemental analyses on $LiFePO_4$/C.

Structural and electrochemical characterization

X-ray powder diffraction (XRPD) patterns were obtained using a D5005 Bruker X-ray diffractometer equipped with Cu-Kα radiation. The accelerating voltage and current were 40 kV and 40 mA, respectively. The scan speed of 0.015° s^{-1} was used. Lattice parameters were obtained using TOPAS-R (version 2.1) software. Scanning electron microscopy (SEM) images were taken from a Jeol JSM-6700F field emission scanning electron microscope (FESEM) operated at 5 kV and 10 mA. For SEM analysis, the samples were coated with a 100-nm-thin platinum coating using DC sputtering. JEOL JEM-2010 was used to get the high-resolution transmission electron microscopy images to study the morphology and measure the carbon layer thickness of the $LiFePO_4$/C nanoplates. For electrochemical studies, composite electrodes were fabricated with the active material, super P carbon black, and binder (Kynar 2801) in the weight ratio 70:15:15 using *N*-methylpyrrolidone as solvent. Electrodes with thickness of 10 μm were prepared using an etched aluminum foil as current collector using doctor-blade technique. Lithium metal foil, 1 M $LiPF_6$ in ethylene carbonate, diethyl carbonate (1:1 *V*/*V*; Merck), and Celgard 2502 membrane were used as counter electrode, electrolyte, and separator, respectively, to assemble coin-type cells (size 2016) in Ar-filled glove box (MBraun, Germany). The geometrical area of the electrode was 2.0 cm^2. Details of cell fabrication have been described previously [20]. The active material content in the electrode was around ~2 mg. The cells were aged for 12 h before the measurement. Charge/discharge cycling at constant current mode was carried out using a computer-controlled Arbin battery tester (Model, BT2000, USA).

Result and discussion

Recently, various synthesis routes such as sol-gel [21, 22], hydrothermal [23], carbothermal [24], polyol method [25], coprecipitation [26, 27], freeze-drying [28], and microwave hydrothermal method [29–32] have been adopted to synthesize nanostructured $LiFePO_4$/C composite and to improve rate performance. Here, we adopt solvothermal method for synthesis of $LiFePO_4$, $LiMnPO_4$, and $LiFe_{0.5}Mn_{0.5}PO_4$ nanoplates.

$LiFePO_4$/C nanoplates were synthesized using solvothermal route [20]. The XRPD studies show single-phase formation of $LiFePO_4$ as seen in Fig. 1. All the peaks in the XRPD pattern were indexed with an orthorhombic space group, *Pnma*. The obtained lattice parameters of $LiFePO_4$/C are a=10.3317 Å; b=6.0083 Å; c=4.6946 Å, and the cell parameters compare well with those reported in the literature (JCPDS Card No. 83-2092).

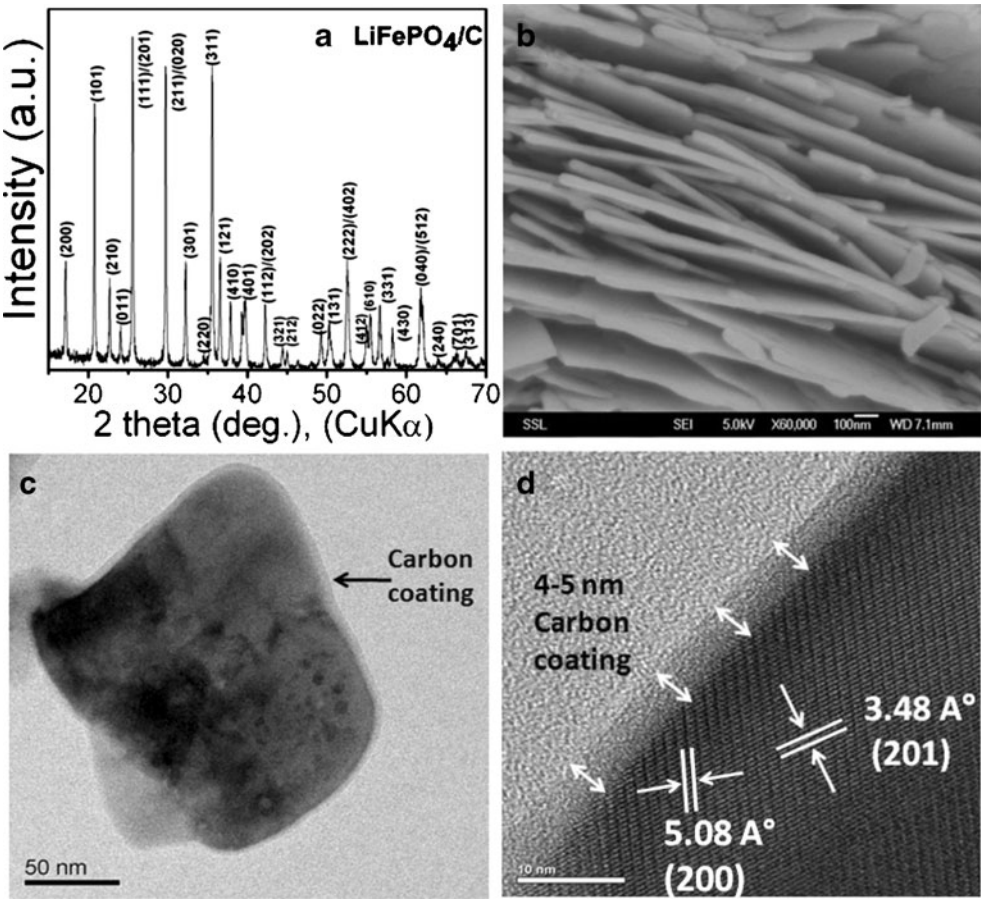

Fig. 1 **a** XRPD pattern of $LiFePO_4$/C nanoplates, **b** FESEM image of the $LiFePO_4$/C nanoplates, **c** TEM image showing a uniform coverage of amorphous carbon coating around the $LiFePO_4$ surface, **d** high-resolution TEM image showing 5-nm-thick amorphous carbon layer around the surfaces of $LiFePO_4$

Further, FESEM and transmission electron microscopy (TEM) techniques were used to characterize the morphology and thin layer of carbon coating on the surfaces of the crystallites. Figure 1b–d presents the FESEM and TEM images of $LiFePO_4$ nanoplates obtained from the solvothermal method. Figure 1b reveals that $LiFePO_4$ plates are with thicknesses of 30–40 nm. Figure 1c, d shows a uniform carbon coating with a thickness of 2–5 nm on $LiFePO_4$ nanoplates in contrast to other reports, where $LiFePO_4$ particles were synthesized by sol-gel method with nonuniform conductive carbon coating [7].

Figure 2a, b is the TEM image and SAED pattern of $LiFePO_4$ nanoplate, respectively. The SAED pattern, same as the [010] SAED pattern of $LiFePO_4$ reported by the Chen et al. [33], reveals that the plate is a $LiFePO_4$ single crystal with *b*-axis along the thinnest direction. The c^*/a^* ratio in the reciprocal lattice from Fig. 2b is found to be 2.20, identical to the a/c ratio of a $LiFePO_4$ crystal with a=1.0334 nm, b=0.6002 nm, and c=0.4695 nm. The large face of the plate (Fig. 2a) lies in the *ac* plane, and its normal is along the *b* direction. It is found that the thickness along the *a*- and *c*-axes is in the range 500–800 nm and 30–40 nm along the *b*-axis (average values based on measurements of about 30 crystallites). It is worth mentioning that the 30–40-nm-thick *b*-axis has been achieved through this solvothermal method.

Raman spectroscopy is a predominantly useful tool for analyzing the coated carbon on the near surface, especially at the D and G bands of carbon [34–36]. Figure 3 shows a characteristic Raman spectrum of $LiFePO_4$/C nanoplates synthesized by solvothermal method. A small band appears at 940 cm^{-1} and is attributed to the symmetric stretching mode of PO_4^{3-} anion in $LiFePO_4$. Two broad and strong bands situated at 1,378 and 1,592 cm^{-1} are designated to the D (disordered) and G (graphene) bands of the residual carbon coated on the $LiFePO_4$ nanoplates, respectively [37–39]. Raman spectra of the $LiFePO_4$/C nanoplates are consistent with earlier reports. The relative intensity ratio between the D and G bands can be used to assess the content of sp^3 and sp^2 carbon in the sample, in addition to the extent of carbon disorder in microcrystalline graphite. Doeff et al. [40–42] reported that increased amounts of sp^2-type carbon or decreased D/G ratio greatly enhance the electronic conductivity, leading to the good discharge capacities and superior rate capability of $LiFePO_4$ cathodes. The I_D/I_G ratios of the $LiFePO_4$ nanoplates are found to be 0.781; this shows the larger amount of graphene clusters than the disordered carbon structure, which facilitates a better cell performance of $LiFePO_4$/C nanoplates as seen from Fig. 4 discussed in later section.

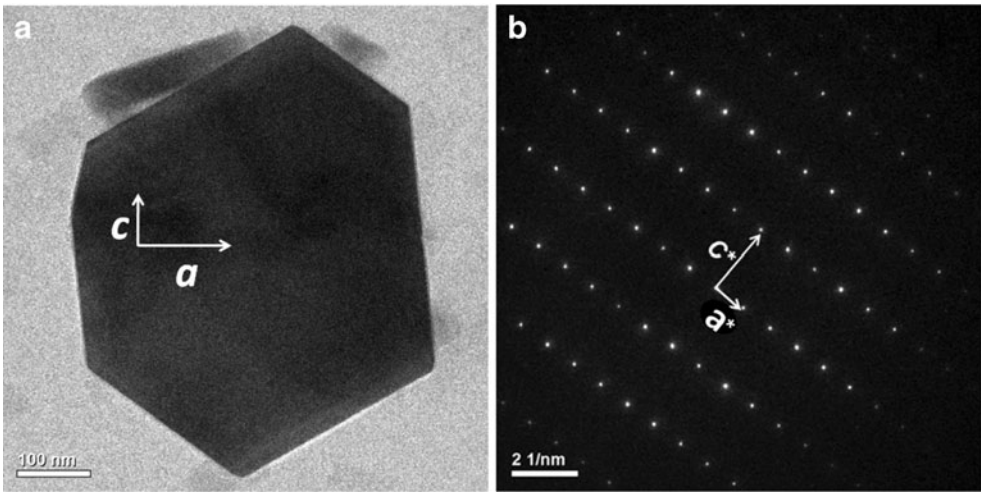

Fig. 2 **a** TEM image of the $LiFePO_4$/C plate with the *a* and *c* directions indicated and **b** the SAED pattern of the nanoplate

Charge–discharge electrochemical performance of a typical $LiFePO_4$/C versus Li cell is shown in Fig. 4 up to 50 cycles at a current density of 17 mA g^{-1} (0.1 C rate) in the voltage range 2.3–4.3 V. During the first-charge (Li deintercalation) process, the voltage increased sharply to ~3.45 V from the open-circuit voltage (OCV=3.0 V) followed by a long plateau until about 125 mAh g^{-1} (Fig. 4a) and then gradually increased to the cutoff voltage value, resulting in a storage capacity of 165 mAh g^{-1} (quite close to the theoretical value of 170 mAh g^{-1}). The discharge curve shows a similar plateau region. The irreversible capacity loss between the first-charge and first-discharge reaction is only about 10 mAh g^{-1}. Quite less polarization of about 60 mV (ΔV) between two plateaus has been observed (Fig. 4a)

It is seen from Fig. 4b that the specific discharge capacities at the end of tenth cycle are 165 (±5) mAh g^{-1} at 0.1 C rate (17 mA g^{-1}) and ~ 46 (±5) mAh g^{-1} at 30 C rate (5,100 mA g^{-1}). These results are much better than those presented earlier by Dominique et al. [3] on $LiFePO_4$/C

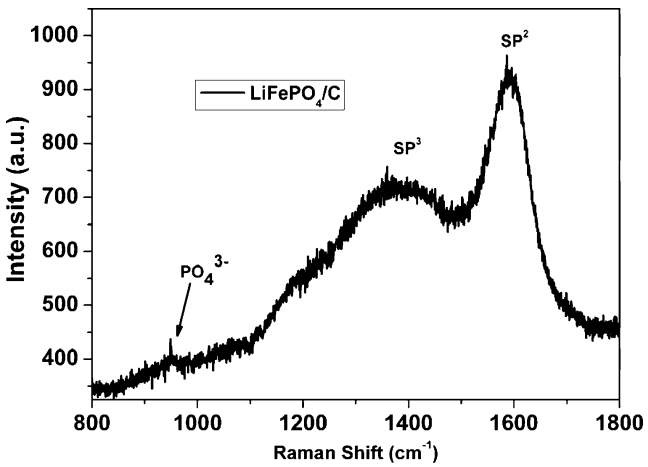

Fig. 3 Raman spectrum of the $LiFePO_4$/C nanoplate

electrode material synthesized using sol-gel method and are very well in agreement with the results reported by Hu et al. [7] using $LiFePO_4$ coated with carbon as well as RuO_2 coating layers. It is worth mentioning that the present solvothermal synthesis approach allows us to avoid expensive RuO_2 coating to achieve high rate performance of $LiFePO_4$.

The above results emphasize the need for optimizing the morphology and hence controlling the thickness of the *b*-axis along which Li^+ ion diffuses fast. Also, the present study highlights the necessity for the carbon coating on the surfaces of $LiFePO_4$. Such an ideal morphology results in a quite high performance at 30 C with a storage capacity of 46 mAh g^{-1}. While dealing with spherical particles of say our own ball-milled $LiFePO_4$, it is clear that the poor performance is due to lack of uniform carbon coating. Although the ball-milled spherical samples have an ideal size of about 40–50 nm, favorable for the fast insertion and extraction of both Li^+ and e^- into the bulk, it does not help in improving the electrochemical performances as the electronic conduction is still low enough to establish a highly conducting surface connectivity with neighboring particles. Thus, it is important to optimize not only the morphology but also conductive carbon surface coating in order to achieve a high rate performance of this cathode material.

Figure 5a, d shows the XRPD patterns of $LiMnPO_4$/C and $LiFe_{0.5}Mn_{0.5}PO_4$/C. XRPD patterns clearly reveal the single-phase formation of $LiFe_{1-x}Mn_xPO_4$ (x=1 and 0.5) nanoplates. All the peaks in the XRPD patterns were well indexed to the corresponding JCPDS pattern (see Fig. 5a, d). Unlike LFP, nanoplates of LMP are not self-assembled and are randomly oriented which is shown in Fig. 5b. The galvanostatic charge and discharge curves of $LiMnPO_4$/C and nanoplates at C/10 are shown in Fig. 5c. LMP nanoplates show a reversible discharge capacity of 47±5 mAh g^{-1}, which is equivalent to 27% of the theoretical capacity of

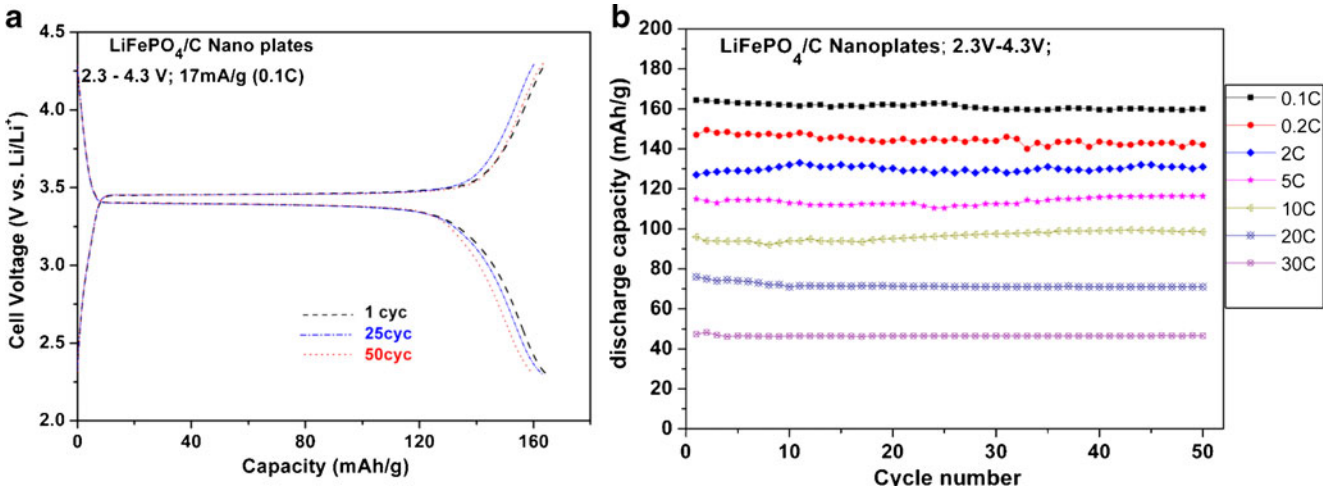

Fig. 4 Galvanostatic charge–discharge cycling curves for $LiFePO_4$ (current density 17 mA/g; potential window 2.3–4.3 V): **a** solvothermal method with carbon coating, **b** rate performance of $LiFePO_4$/C (here 1 C refers to a capacity of 170 mA/g in 1 h)

171 mAh g^{-1} of LMP. These galvanostatic charge–discharge results are comparable to that reported earlier [43–46]. This restricted electrochemical performance could be the result of very less intrinsic electronic conductivity and sluggish lithium diffusion kinetics within the LMP plates. In addition, the poor performance of LMP during discharge is attributed to the poor mechanical strength of the nanoplates upon Li insertion. On the other hand, LMP nanoplates prepared by Wang et al. [47] using polyol method performs well upon ball milling with carbon precursor. When compared with LMP/C, solid-solution $LiFe_{0.5}Mn_{0.5}PO_4$/C nanoplates exhibit a better storage performance of 65±5 mAh g^{-1} with very less irreversible capacity loss under similar conditions. It is quite interesting to note that the mechanical strength of the nanoplates has improved in the $LiFe_{0.5}Mn_{0.5}PO_4$, similar to $LiFePO_4$. Even the morphologies of $LiFePO_4$ and $LiFe_{0.5}Mn_{0.5}PO_4$ look quite similar with self-assembly of nanoplates (see Figs. 1b and 5e) whereas $LiMnPO_4$ forms isolated nanoplates (Fig. 5b). Thus, the morphology of $LiFe_{1-x}Mn_xPO_4$/C (x=0, 0.5, and 1) is found to be sensitive to their high storage performance.

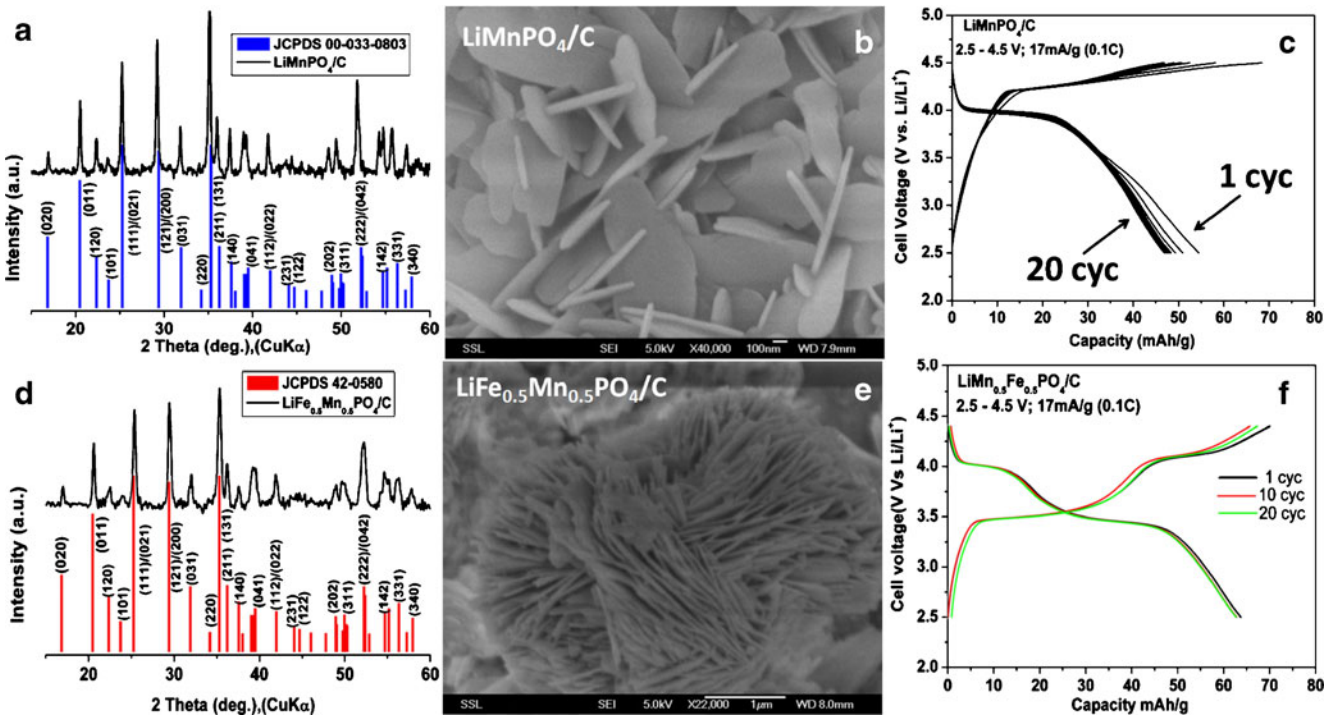

Fig. 5 $LiMnPO_4$/C nanoplates: **a** PXRD pattern, **b** FESEM image with *scale bar* 100 nm, and **c** galvanostatic charge–discharge cycling curves. $LiFe_{0.5}Mn_{0.5}PO_4$/C nanoplates: **d** PXRD pattern, **e** FESEM image with *scale bar*, 1 μm, **f** galvanostatic charge–discharge cycling curves

Conclusion

We have synthesized nanoplates of $LiFePO_4$ with 5-nm-thin uniform carbon coating by solvothermal method, and also we have extended the synthetic strategy to prepare the nanoplates of $LiMnPO_4$/C and $LiFe_{0.5}Mn_{0.5}PO_4$/C. The thickness along the *b*-axis is found to be 30–40 nm in case of $LiFePO_4$/C, such morphology favors short diffusion lengths for Li^+ and e^-, resulting in high rate performances. Thus, we have demonstrated that the Li^+ diffusion along the *b*-axis and conductive surface coating are crucial for the high rate storage performances of $LiFePO_4$/C as cathode materials in lithium-ion batteries in the light of present demands for high-power applications such as electrical vehicle and power tools.

Acknowledgements We thank the Ministry of Education, Singapore, for funding through NUS FRC Grant No. R143-000-283-112 and FRC Grant No. R265-000-274-133. The authors also thank Dr. Nagarathinam Mangayarkarasi, NUS for their valuable comments, and Dr. Sudip Batabyal, Department of Chemistry, NUS for help in SEM analysis. Saravanan would like to thank NUS for the NUSNNI Graduate Scholarship.

References

1. Padhi AK, Nanjundaswamy KS, Goodenough JB (1997) J Electrochem Soc 144:1188–1194
2. Chung SY, Blocking JT, Ching YM (2002) Nat Matters 1:123–128
3. Herle PS, Ellis B, Coombs N, Nazar LF (2004) Nat Matters 3:147–152
4. Rousse G, Carvajal JR, Patoux S, Masquelier C (2003) Chem. Mater Des 15:4082–4090
5. Yamada A, Koizumi H, Nishimura SI, Sonoyama N, Kanno R, Yonemura M, Nakamura T, Kobayashi Y (2006) Nat Matters 5:357–360
6. Andersson AS, Thomas JO (2001) J Power Sources 97–98:498–502
7. Hu YS, Guo YG, Dominko R, Gaberscek M, Jamnik J, Maier J (2007) Adv. Mater Des 19:1963–1966
8. Ravet N, Abouimrane A, Armand M (2003) Nat Matters 2:702
9. Ojczyk W, Marzec J, Wierczek KS, Zajac W, Molenda M, Dziembaj R, Molenda J (2007) J Power Sources 173:700–706
10. Delacourt C, Laffont L, Bouchet R, Wurm V, Leriche JB, Morcrette M, Tarascon JM, Masquelier C (2005) J Electrochem Soc 152:A913–A921
11. Amin R, Balaya P, Maier J (2007) Electrochem Solid-State Lett 10:A13–A16
12. Morgan D, Van der Ven A, Ceder G (2004) Electrochem Solid-State Lett 7:A30–A32
13. Maxisch T, Zhou F, Ceder G (2006) Phys Rev B 73:104301–104306
14. Islam MS, Driscoll DJ, Fisher CAJ, Slater PR (2005) Chem Mater 17:5085–5092
15. Fisher CAJ, Islam MS (2008) J Mater Chem 18:209–1215
16. Huang H, Yin SC, Nazar LF (2001) Electrochem Solid-State Lett 4:A170–A172
17. Chen Z, Dahn JR (2002) J Electrochem Soc 149:A1184–A1189
18. Moskon J, Dominko R, Korosec RC, Gaberscek M, Jamnik J (2007) J Power Sources 174:683–688
19. Ait Salah A, Mauger A, Zaghib K, Goodenough JB, Ravet N, Gauthier M, Gendron F, Julien CM (2006) J Electrochem Soc 153:A1692–A1701
20. Saravanan K, Reddy MV, Balaya P, Gong H, Chowdari BVR, Vittal JJ (2009) J Mater Chem 19:605–610
21. Dominko R, Bele M, Gaberscek M, Remskar M, Hanzel D, Goupil JM, Pejovnik S, Jamnik J (2006) J Power Sources 153:274–280
22. Gabersceka M, Dominko R, Bele M, Remskar M, Hanzel D, Jamnik J (2005) Solid State Ionics 176:1801–1805
23. Yang S, Zavaliji PY, Wittingham MS (2001) Electrochem Commun 3:505–508
24. Barker J, Saidi MY, Swoyer JL (2003) Electrochem Solid-State Lett 6:A53–A55
25. Kim DH, Kim J (2006) Electrochem Solid-State Lett 9:A439–A442
26. Delacourt C, Poizot P, Levasseur S, Masquelier C (2006) Electrochem Solid-State Lett 9:A352–A355
27. Arnold G, Garche J, Hemmer R, Strobele S, Vogler C, Mehrens MW (2003) J Power Sources 119–121:247–251
28. Palomares V, Goni A, Muro IGD, Meatza ID, Bengoechea M, Miguel O, Rojo T (2007) J Power Sources 171:A484–A487
29. Manthiram A, Vadivel Murugan A, Sarkar A, Muraliganth T (2008) Energy Environ Sci 1:621–638
30. Vadivel Murugan A, Muraliganth T, Manthiram A (2008) Electrochem Commun 10:903–906
31. Vadivel Murugan A, Muraliganth T, Manthiram A (2009) Inorg Chem 48:946–952
32. Bilecka I, Hintennach A, Djerdj I, Novak P, Niederberger M (2009) J Mater Chem 19:5125–5128
33. Chen G, Song X, Richardson TJ (2006) Electrochem Solid-State Lett 9:A295–A298
34. Tanabe Y, Yamanaka J, Hoshi K, Migita H, Yasuda E (2001) Carbon 39:2347–2353
35. Sadezky A, Muckenhuber H, Grothe H, Niessner R, Pöschl U (2005) Carbon 43:1731–1742
36. Song SW, Reade RP, Kostecki R, Striebel KA (2005) J Electrochem Soc 153:A12–A19
37. Kuo Fey GT, Lu TL, Wu FY, Li WH (2008) J Solid State Electrochem 12:825–833
38. Lua CZ, Feya GT, Kao HM (2009) J Power Sources 189:155–162
39. Maccario M, Croguennec L, Desbat B, Couzi M, Cras F, Le Servantd L (2008) J Electrochemical Society 155:A879–886
40. Doeff MM, Hu Y, McLarnon F, Kostecki R (2003) Electrochem Solid State Lett 6:A207–A209
41. Doeff MM, Wilcox JD, Kostecki R, Lau G (2006) J Power Sources 163:180–184
42. Hu Y, Doeff MM, Kostecki R, Finones R (2004) J Electrochem Soc 151:A1279–A1285
43. Delacourt C, Poizot P, Morcrette M, Tarascon JM, Masquelier C (2004) Chem Mater 16:93–99
44. Yamada A, Kudo Y, Liu K (2001) J Electrochem Soc 148:A1153–A1158
45. Vadivel Murugan A, Muraliganth T, Manthiram A (2009) J Electrochem Soc 156:A79–A83
46. Fang H, Li L, Yang Y, Yan G, Li G (2008) Chem Commun 1118–1120
47. Wang D, Buqa H, Crouzet M, Deghenghi G, Drezen T, Exnar I, Kwon NH, Miners JH, Poletto L, Graetzel M (2009) J Power Sources 189:624–628